Arch. Metall. Mater. **65** (2020), 4, 1405-1415

DOI: 10.24425/amm.2020.133707

Z. MIKNO[1*], M. STĘPIEŃ[2], B. GRZESIK[2]

NUMERICAL MODELLING AND MEASUREMENTS OF TEMPERATURE FOR TESTS OF STRUCTURAL TRANSFORMATIONS IN STEELS UNDER WELDING CONDITIONS

This paper presents the way in which temperature is measured in tests concerning structural transformations in various types of steel under welding conditions. In the test methodology, a small-sized steel specimen was subjected to simulated welding thermal cycles, during which the temperature of the specimen, changes in magnetic permeability and thermal expansion were measured simultaneously. The measurements of those parameters required the non-contact heating of the specimen, which involved the use of heating lamps. The temperature measurement was of key importance because the subsequent analysis of the remaining parameters was performed in the function of temperature.

The tests of structural transformations resulted in the development of Continuous Cooling Transformation under welding conditions (*CCT*) diagrams, enabling the determination of steel weldability and constituting the source of information needed to determine the effect of welding thermal cycles on the structure and properties of the material subjected to the tests.

Related numerical models to be used as the basis for the analysis of temperature distribution in the test specimen have been developed. These tests involved the analysis of the values and the distribution of temperature in relation to various model parameters, i.e. thermocouple types, geometrical features of a thermocouple junction and the diameter of thermocouple wires. The results of FEM calculations have been compared to the experiments.

Keywords: FEM; thermocouple measurement, *CCT* diagrams

1. Introduction

The weldability of steel is determined using diagrams of austenite decomposition, i.e. Continuous Cooling Transformation under welding conditions (*CCT*). The above-named diagrams constitute the source of vitally important information concerning the effect of welding thermal cycles on the structure and properties of various types of steel and, among other things, enable the optimum design of technologies dedicated to joining steel elements in a manner allowing the best possible properties of welded joints to be obtained and, as a result, the highest possible crack resistance of entire structural elements to be achieved [1].

Until today, a number of methods have been developed to allow the determination of the weldability of steels. The easiest way to assess the steel weldability is to use empirical formulas for carbon equivalent (CE), which contain elements of the chemical composition of steel [2]. However, it is not sufficient to determine the specific properties of welded joints. Therefore, it is necessary to reproduce, as closely as possible, special conditions present during weld fabrication. This means reproducing [3]:

- joint configuration (fillet or groove, groove type, etc.),
- degree of inherent restraint as imposed by the base material thickness or general mass,
- degree of imposed restraint from fixtures or other elements of the test rig.

No single test can be expected to measure all of the aspects of the complex properties of welded joints. The most popular tests are Y-groove (Tekken) and U-groove tests [4]. The Tekken test is a more restrictive test if compared to the U-groove test. From a practical point of view, the Tekken test is a better solution as a criterion for estimating the preheating temperature. Although many practical tests can be used to assess the weldability of metals, the physical simulation techniques are still popular and useful [5]. The physical simulation in thermal stress cycle simulators can be carried out. The main concept of the thermal-mechanical simulator is simple, i.e. electric current flows through the specimen and the Joule heat generates the heat flow from

[1] ŁUKASIEWICZ RESEARCH NETWORK – INSTITUTE OF WELDING, DEPARTMENT FOR RESISTANCE WELDING, ADHESIVE BONDING, ENVIRONMENTAL PROTECTION, BL. CZESLAWA 16-18, 44-100, GLIWICE, POLAND
[2] SILESIAN UNIVERSITY OF TECHNOLOGY, FACULTY OF ELECTRICAL ENGINEERING, KRZYWOUSTEGO 2, 44-100 GLIWICE, POLAND

* Corresponding author: Zygmunt.Mikno@is.gliwice.pl

the centre of the specimen towards cold copper jaws, producing real temperature gradients [6]. Based on the thermomechanical simulation it is possible to estimate the toughness as well as the hardness of simulated HAZ (heat affected zone). However, in order to determine the cooling rate of these steels in the HAZ, it is necessary to analyse the cooling conditions in this zone. This is possible on the basis of Continuous – Cooling – Transformation diagrams for welding conditions. The above-named diagrams constitute the source of vitally important information concerning the effect of welding thermal cycles on the structure and properties of various types of steel and, among other things, enable the optimum design of technologies dedicated to joining steel elements in a manner allowing the best possible properties of joints to be obtained and, as a result, the highest possible crack resistance of entire structural elements to be achieved [1,7].

The determination of *CCT* diagrams requires the knowledge of critical temperatures (i.e. of the beginning and end) of structural transformations occurring in solid-state steels during heating and cooling. The precise identification of critical temperatures determining the beginning and end of structural transformations in steel during welding thermal cycles requires appropriate testing methodology and measuring equipment [1]. The accuracy of measured parameters is very important since it can be used for the determination of numerical models of *CCT* [8].

The test rig described in the article is unique because of the fact that the related measurement methodology is based on simultaneous measurements of three measurement parameters, i.e. the temperature of the material being tested (specimen) as well as its thermal expansion and changes in magnetic permeability. The tests utilise three methods, i.e. dilatometric, magnetometric and thermal analysis. The above-named accuracy is significantly higher than that obtained on the basis of one phenomenon, usually thermal expansion [9-11] or temperature, and tests of a material subjected to a thermal cycle [12,13].

The in-depth knowledge of phenomena taking place in solid-state type steels makes it possible, among other things, to forecast the types of metallographic structures formed depending on various parameters of thermal cycles, which, in turn enables the forecasting of the mechanical and plastic properties of these steels, critical for the operational properties of structural elements [1].

The knowledge about weldability including *CCT* diagrams and the accuracy of temperature measurement used in the testing methodology directly affect the quality of welds and, consequently, the safety of welded structures. This aspect is particularly important with respect to the making of welded joints in critical supervised elements, the quality of which affects human life and or health and the damage to which could cause significant material losses [14,15].

This article discusses the optimisation of the thermocouple-based measurement of temperature applied in a device used for the determination of *CCT* diagrams for welding conditions. The welding technology developed on the basis of these diagrams significantly affects both the quality and the safety of welded structures. The improvement of the device functionality included a considerable increase in temperature measurement accuracy, significantly affecting the accuracy of the determination of *CCT* diagrams for welding conditions. The methodology of the thermocouple-based measurements of temperature was analysed using an FEM-based computational model and was subjected to experimental verification.

TABLE 1

List of abbreviations used in the text

Abbreviation	Description
CCT	Continuous Cooling Transformation *under welding conditions*
FEM	Finite Element Method
VTT	volume-type thermocouple
STT	surface-type thermocouple
T	desirable temperature measurement
T_T	actual temperature measurement area
N_T	time constant determines the dynamic properties of thermocouple junctions
PtRh10-Pt	thermocouple type “S” (platinum 90%, rhodium 10%)
NiCr-NiAl	thermocouple type “K” (nickel-chromium / nickel-aluminium),
T*J-00X*	*T* – thermocouple *J* – junction type (S – surface type, V – volume type) 00 – sensor wire diameter in micrometres *X* – sensor type {**K** – NiCr-NiAl, **S** – PtRh10-Pt}
TS	surface thermocouple
TV	volume thermocouple
TV-200K	(TV) volume thermocouple, (200) wire diameter ϕ = 200 μm, (K) thermocouple type “K”
TS-200S	(TS) surface thermocouple, (200) wire diameter ϕ = 200 μm, (S) thermocouple type “S”
TS-50S	(TS) surface thermocouple, (50) wire diameter ϕ = 50 μm, (S) thermocouple type “S”
TS-200K	(TS) surface thermocouple, (200) wire diameter ϕ = 200 μm, (K) thermocouple type “K”
TS-50K	(TS) surface thermocouple, (50) wire diameter ϕ = 50 μm, (K) thermocouple type “K”
800-500°C	temperature range
$T_{8\text{-}5}$	abbreviation of temperature range (800-500°C),
$t_{8/5}$	time at which temperature during cooling changes within the range of 800°C to 500°C
T_2	analysed temperature (FEM) on the tested sample where the thermocouple was located (welded), point 2 Fig. 3
T_3	analysed temperature (FEM) on the tested sample where the thermocouple was not present physically, point 2 Fig. 5

2. Methodology of the experiment

2.1. Structure of the test rig and the methodology of measurements

The primary elements of the test rig are presented in Figure 1. The testing methodology involved subjecting the test specimen to simulated welding thermal cycles. The test speci-

men (1) was placed on a thermally and magnetically insulated base (2) in a magnetic circuit (3) and was heated by the radiation emitted by heating lamps (4). Magnetic permeability is measured in a magnetic circuit (2), the components of which include a transmitter coil (5) and a receiver coil (6). The expansion of the specimen is measured using a laser sensor (7) recording the movements of the upper pusher (2). The components are located in the housing (8). The heating lamps constituted the source of heat and were used to represent a simulated welding thermal cycle. The use of the lamps as heat sources resulted from the need for supplying heat to the specimen in a non-contact manner ensuring the precise measurement of thermal expansion and magnetic permeability [16]. The power of the heating lamps necessary for heating the specimen to a temperature of 1350°C conditioned the dimensions of the test specimen, the weight of which amounted to approximately 1 gram. The test specimen shape was that of a 6 mm high tube having a diameter of 6 mm. The shape and the weight of the specimen, as well as the thickness of its wall, were also dictated by the necessity of the fast and uniform heating and cooling of the specimen.

The test rig is used to represent the welding thermal cycle. i.e. at a preset time (several seconds) the specimen is heated to the preset maximum temperature. Afterwards, the specimen is cooled at a preset cooling rate. During the thermal cycle the specimen is subjected to heat (1); the change in temperature is accompanied by the expansion or contraction of the specimen as well as by the change in the specimen magnetic permeability.

The tests involve measurements of thermal expansion, magnetic permeability and temperature determined as the function of time [1]. Changes in magnetic permeability are identified by the measurement of voltage induced in a *receiving* coil (secondary winding) magnetically coupled (via the test steel specimen) with a *transmitting coil* (primary winding) powered by direct current. The occurrence of the Curie temperature (magnetic transformation point) triggers the loss or the recovery of the ferromagnetic properties of the steel specimen and, at the same time, the intense change in the magnetic permeability of the circuit. Changes in magnetic permeability are observed not only at the Curie temperature. Smaller changes in magnetic permeability result from structural transformations. The analysis of parameters measured in time is helpful in the analysis of results, yet it is of little use when determining the diagrams of structural transformations. The determination of characteristic points is based on the analysis of primary parameters, i.e. thermal expansion and changes in magnetic permeability, in the function of temperature [17]. The higher-order functions, e.g. the first and the second derivative of the above-named parameters and of temperature itself [18] are also analysed in the function of time. The measurement of temperature is of key importance with respect to the dependence of measured parameters and their further transformations as well as in terms of the analysis in the function of temperature [19]. Another important aspect is the precise measurement of thermal expansion and the change in magnetic permeability being the basis used to determine the characteristic points in the function of temperature.

The small dimensions and the shape of the specimen pose a challenge for the methodology of temperature measurements. According to the authors' experience [19,20], the most favourable is the use of the thermocouple-based measurement of temperature. The experience indicates the necessity of the in-depth analysis of temperature distribution in the test specimen resulting from the heating performed by heating lamps as well as from the use of a thermocouple of specific dimensions, shape and weight [21-23]. The specimen weight-thermocouple weight ratio significantly affects the discharge of heat from areas subjected to measurements, significantly affecting the temperature

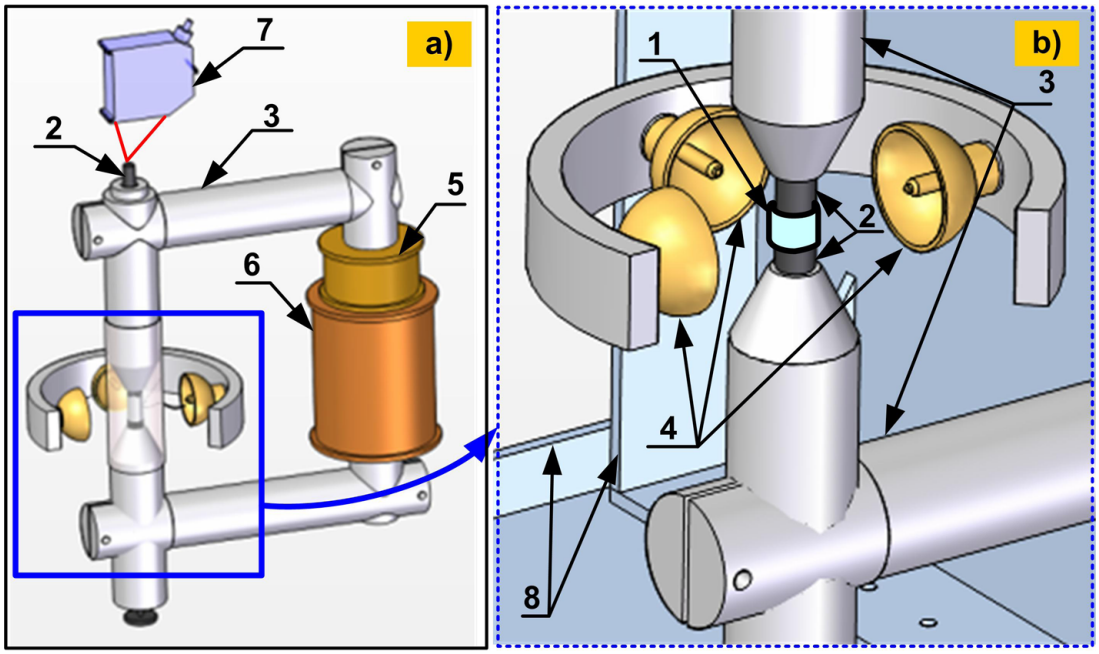

Fig. 1. Test rig for the investigation of phase transformations along with main elements 1) test specimen, 2) thermally and magnetically insulated material, 3) magnetic circuit and 4) heating lamps

at the point of measurement. The determination of temperature measurement uncertainty and the identification of the effect of the thermocouple material and its size on the accuracy of temperature measurements required the development of an appropriate computer-aided FEM model and the performance of related calculations [24].

The investigation carried out in the research, including FEM modelling and measurements, is based on different types of thermocouple sensors labelled in the paper with the general symbol T*J-00X* where *J* refers to the junction type (S- surface type, V – volume type), 00 is a sensor wire diameter in micrometres, and *X* refers to the sensor type ("K" – NiCr-NiAl (K), "S" – PtRh10-Pt (S)).

An important test rig-related aspect was the fact that the specimen was subjected to the blow-in of shielding gas during the heating stage and (in cases of cycles involving fast cooling) to the blow-in of cooling gas during the cooling stage. To provide appropriate gas protection (shielding), the specimen was placed inside a quartz tube.

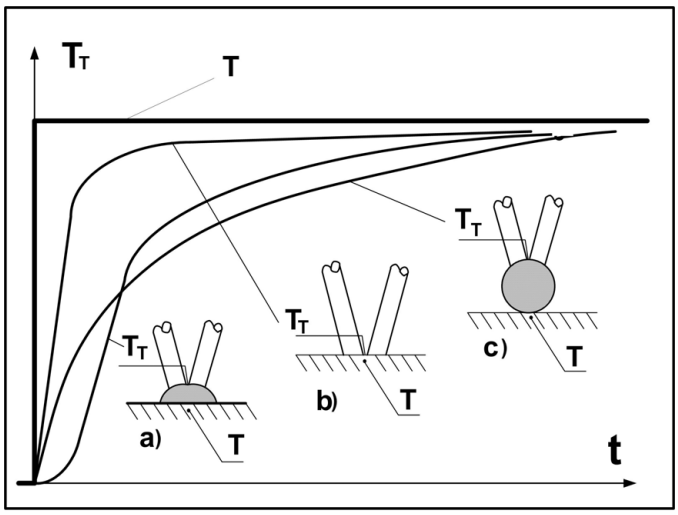

Fig. 2. Course of temperature (signal from the thermocouple) *T* measured during the leap of the temperature of the object being measured near the thermocouple junction T_T in relation to three various thermocouple designs [21]

2.2. Thermocouple properties and preparation

When considering test rig-related solutions concerning temperature measurements, various, preferably non-contact, methods were taken into account. The thermographic or pyrometric method would be the most comfortable, yet impossible to implement successfully because of: the intense flow of (shielding and cooling) gas in the measurement area, the presence of the quartz casing additionally screening the field of temperature measurement and the reflected radiation of heating lamps disrupting the measurements of temperature. The selection of the thermocouple-based solution was dictated mainly by high dynamics of measurements.

The thermocouple-based measurement method was subjected to multi-aspect and multi-criterion optimisation analysis based on numerical and experimental tests aimed at obtaining the most accurate results of temperature measurements. The authors' experience clearly confirmed the direct effect of the shape and design of a thermocouple junction on the results of temperature measurements.

Figure 2 presents the three primary types of thermocouples, e.g. volume, surface and contact type. The preliminary comparative tests involved only two thermocouple types, i.e. a) volume-type (*VTT*) and b) surface-type thermocouple (*STT*). The contact thermocouple was rejected (c) as, in the case under discussion it was burdened with an excessively high dynamic error and could not be practically used on the test rig [21].

The designations adopted in Figure 2: *T* – desirable temperature measurement area and T_T – actual temperature measurement area.

The *VTT* (Fig. 2a) was characterised by the significant volume of the thermocouple junction and the large area where it was welded to the material (in the temperature measurement area). The *STT* (Fig. 2b) was characterised by the zero volume of the thermocouple junction and the smaller contact area (i.e. area in which the thermocouple was welded to the material) in the temperature measurement area. The measurement dynamics of the *STT* proved the most favourable.

Figure 3 presents the scanning microscopic photographs of *VTT* (a) and *STT* (b) junctions welded to the base (material). The diameter of the thermocouple wires amounted to 200 mm.

In the publication [21] the analysis of the shape and design of thermocouple junctions is discussed. The dynamic properties of junctions are determined by the time constant N_T, expressed by the following dependence

$$N_T = \frac{m \cdot c}{\frac{\lambda}{w} \cdot S} = \frac{\gamma \cdot V \cdot c}{\frac{\lambda}{w} \cdot S} = \frac{\gamma \cdot S \cdot w \cdot c}{\frac{\lambda}{w} \cdot S} = \frac{\gamma \cdot w^2 \cdot c}{\lambda} \qquad (1)$$

Where: m – mass, c – specific heat, w – height of the junction, λ – thermal conductivity, S – area of heat exchange (with the material being tested), γ – material density.

As can be seen in dependence (1), the dynamic properties of the thermocouple junction depend on the type of the thermocouple material, i.e. on material parameters (specific heat and thermal conductivity) as well as on the weight and the shape (area of contact with the material being tested and the height) of the thermocouple.

It seems justified to state that in order to minimise the time constant (N_T) of the temperature measurement, the material of the thermocouple should be characterised by high thermal conductivity, low specific heat and the lowest possible weight.

Figure 4 presents the *VTT* welded to the steel sheet using a capacitor welding machine. The thermocouple junctions were made in relation to the same welding technology parameters. Figure 4b reveals the lack of repeatability when making such thermocouple junctions, i.e. different volumes and heights of the thermocouple junctions. In relation to the tests performed using

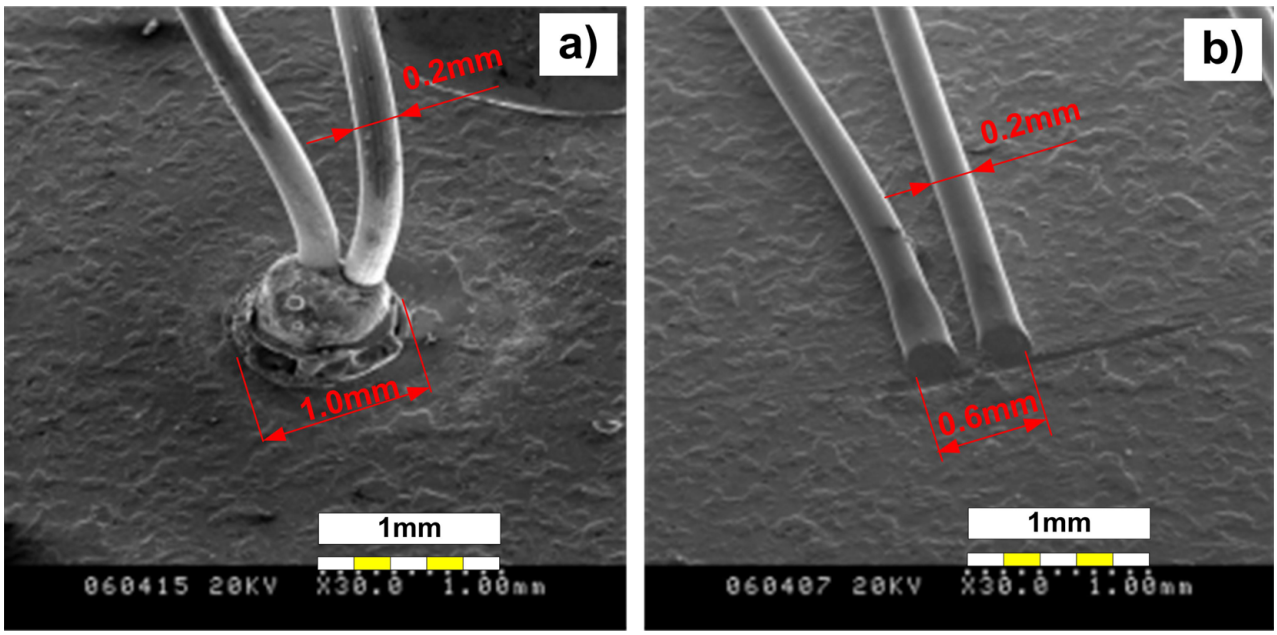

Fig. 3. Thermocouple junctions welded to the base; a) *VTT* and b) *STT*

the test rig as well as constant intensity and time of heating, the differences of temperature indications amounted to 80°C. The lack of thermocouple junction shape repeatability is a factor restricting the use of such a thermocouple type.

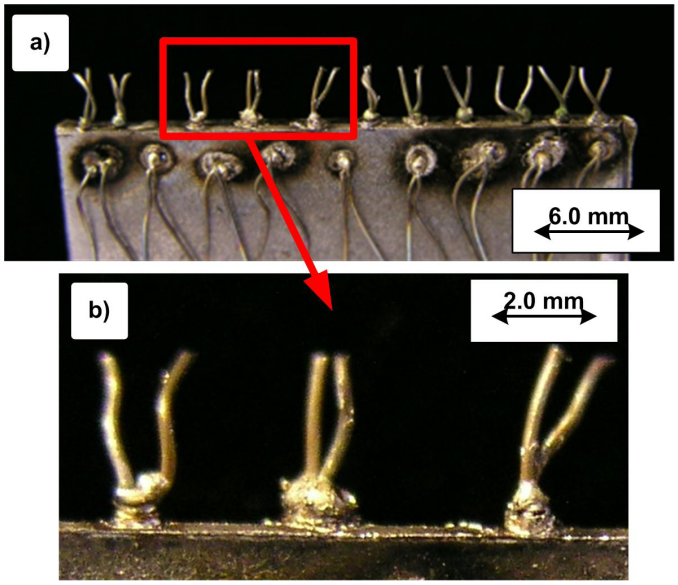

Fig. 4. Magnified *VTT*: a) x1, b) x10 (digital photographs)

It is necessary to pay attention to the effect of individual factors on the measurement of temperature in the case being analysed, i.e. the measurement of temperature in a small-sized element in dynamic transient states. The lower weight of the thermocouple definitely improves the dynamics of temperature measurements, yet the effect of the material parameters on the thermocouple junctions is not so evident. The precise analysis of accuracy of temperature measurements requires the performance of FEM calculations followed by their experimental verification.

3. Numerical analysis

3.1. FEM computational model

The tests involved the analysis of the process of thermal transformations in the specimen using computer-aided analysis based on the FEM method and the ANSYS software programme. The tests involved the use of the FEM – 3D model for both the specimen and the thermocouple. In terms of geometry, the entire computer model contained approximately 60 000 finite elements and approximately 20.000 nodes. The computer model was based on the SOLID 70 type finite elements predefined in the ANSYS software programme. The above-named elements were tretrahedral elements of the first order used in thermal analysis (of steady states and transient processes) oriented in the Cartesian coordinate system. The simulations were carried out using equations based on the first law of thermodynamics (2) combined with Fourier's law (3).

$$\rho c \frac{dT}{dt} + \{L\}^T \{q\} = \ddot{\dot{q}} \tag{2}$$

$$\{q\} = -[D]\{L\}T \tag{3}$$

where ρ – density, c – specific heat, T – temperature, t – time, $\{L\}$ – vector operator, $\{q\}$ – heat flux vector, $\ddot{\dot{q}}$ – heat generation transferred by the radiation, $[D]$ – conductivity matrix.

The geometry of the model is presented in Figure 5. The figure presents the geometry of the model along with the mesh of finite elements, the area through which radiation penetrated both the specimen (one of four areas) and the temperature recording points. It relates also to boundary conditions defined in the model. The model included: i) four heat point sources (presented in Fig. 5; only for heating period) set by the first type boundary condition as constant temperature (of 2500°C), ii) emissivity

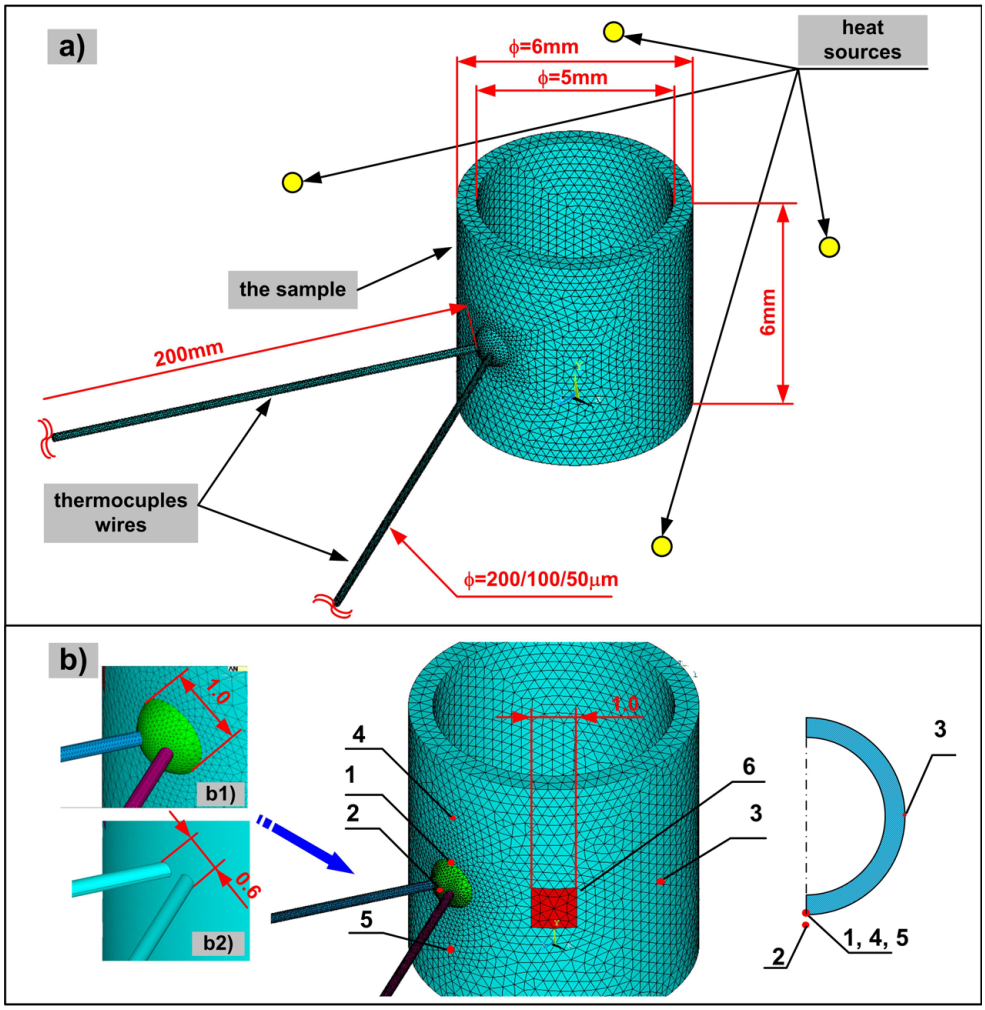

Fig. 5. Geometrical model: a) entire model with the heating sources (lamps) and the thermocouple, b) test specimen with the temperature recording points (1-5), radiation penetration area (6) and various thermocouple types

coefficient as boundary condition set on four heated surfaces of the sample (marked as red rectangles in Fig. 5); emissivity was defined experimentally for a given steel type in order to obtain proper trajectory of heating profile, iii) ambient temperature as the first type boundary conditions set at the thermocouple ends (20°C); iv) heat flux removal coefficient defined for all sample surfaces (except heating surfaces during heating period); values of the coefficient depended on cooling type (free cooling or forced gas cooling); for free cooling the heat flux has been defined as 500 W/(m×K).

The analysis involved both the *VTT* and the *STT*.

The computer models were made in relation to several specimens. The basic specimen dimensions included the height amounting to 6 mm, the external diameter amounting to 6 mm and the wall thickness amounting to 0.5 mm.

The tests were based on the analysis of thermal transient states in the model. The excitation was performed by determining the temperature difference between the sources of radiation (constant temperature in the entire cycle) and the test specimen (temperature preset at the beginning of the process of heating). The tests were performed for thermal cycles not exceeding 20 sec. with a computational resolution of 0.1 sec.

3.2. FEM calculations

The developed model involved the performance of various numerical calculations. The results are related to a number of different variants including: i) types of thermocouples (volume or surface-type), ii) thermocouple materials (PtRh10-Pt or NiCr-NiAl), iii) thermocouple wire diameters (50 and 200 mm), iv) rate of the specimen cooling cycle (natural and fast cooling), v) test specimen wall thickness and vi) test specimen material.

The analyses led to the development of space distributions of temperature in the specimen and in the thermocouple wires and, in particular, in five characteristic points on the external surface of the specimen (Figure 5):

– at the halfway point of the specimen height (point 1),
– between thermocouple wires (in relation to the *VTT*) (point 2),
– at the halfway point of the distance between neighbouring heat sources and at the halfway point of the specimen height (point 3),
– at ¼ (point 5) and ¾ (point 4) of the specimen height.

The calculations were performed in relation to *K-type* thermocouples welded to the specimen, in relation to three design variants (Fig. 6): 1) TS-50K, 2) TV-200K, 3) TS-200K.

In the related range of temperature changes (i.e. 800-500°C), the differences of indications amounted to approximately 74°C (Fig. 6a) in relation to the *VTT*. The model revealed the effect of the weight and type of individual thermocouples on the distribution of temperature in the specimen (Fig. 6a-c). The temperature indications strongly depended on the above-presented factors.

Figure 7 presents the results of the analysis in relation to the thermocouple, thermocouple wires and the inside of the thermocouple wires. It is possible to notice the effect of the thermocouple on the distribution of temperature in the specimen, particularly in the area where the thermocouple is welded to the

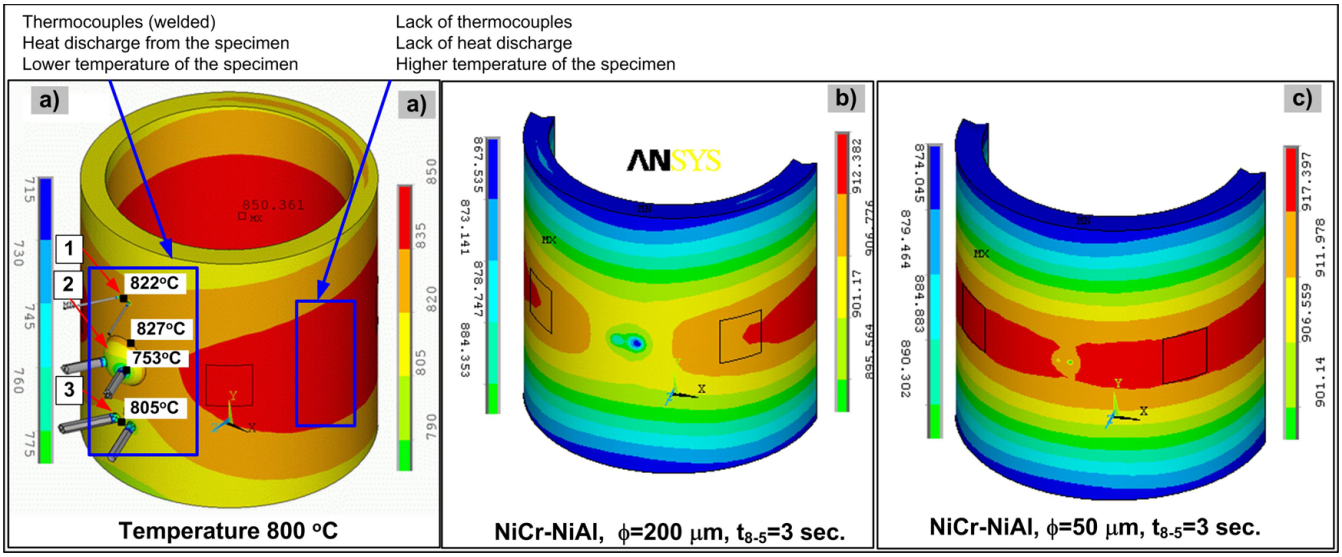

Fig. 6. The temperature distribution on the specimen in relation to: a) three different types of sensors welded to one specimen, b) TS-200K, c) TS-50K

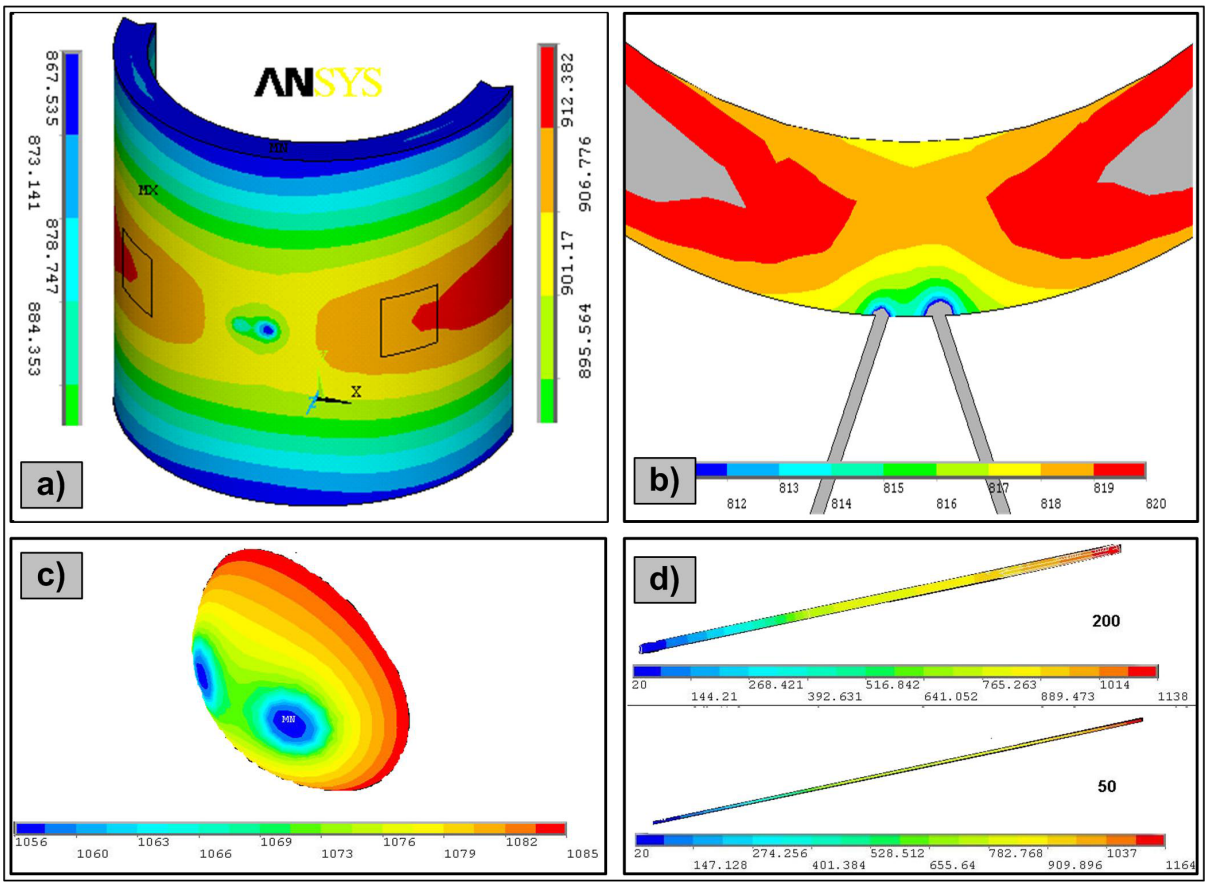

Fig. 7. The distribution of temperature in the temperature measurement area in relation to: a) entire specimen, b) TS-type sensor, c) TV-type sensor and d) sensor wires (ϕ = 200 μm i 50 μm)

steel specimen. Obviously, the foregoing affects the measurement of temperature performed using the thermocouple. The model also allowed for the material parameters of thermocouple wires, i.e. their thermal conductivity and specific heat. The above-named parameters varied depending on thermocouple wires. The effect is visible in Figure 7a, i.e. as different values of temperature in the areas where the thermocouple wires are welded to the specimen.

Figure 8 presents the course of temperature in the function of time in relation to various points of analysis. Figure 8a1/b1 presents the course of temperature in relation to the entire cycle of heating and cooling, Figure 8a2/b2 presents the course of temperature at the time of cooling within the temperature range of 800°C to 500°C ($T_{8\text{-}5}$) and Figure 8a3/b3 presents the difference of temperature values at the time of cooling within the $T_{8\text{-}5}$. The thermocouple type is a parameter in the results. The analysis involved different thermocouples: TS-50S, TS-200S and TS-200K.

The calculations presented in Figure 8a, were performed in relation to two diameters of thermocouple wires, i.e. 50 mm and 200 mm. The analysis involved the process of heating (3 sec.) and fast cooling ($t_{8\text{-}5}$ = 3 sec). The diameters of thermocouple wires affected the discharge of heat from the specimen area to which the thermocouple was welded and directly affected the absolute value of temperature being measured. The maximum difference in temperature indications within the $T_{8\text{-}5}$ amounted to 31°C. The above-named value changed within the $T_{8\text{-}5}$.

As shown in the results presented in Figure 8b, calculations were performed in relation to two thermocouples: TS-200K and TS-200S. Because of the greater thermal conductivity of thermocouple PtRh10-Pt, heat is discharged more intensively from the test specimen, thus reducing the specimen temperature, particularly in the area of measurement. Within the $T_{8\text{-}5}$, the maximum difference amounted to 8,5°C (Fig. 8c). Greater temperature indications were observed in relation to the thermocouple characterised by the lower thermal conductivity. In order to improve the accuracy of specimen temperature determination (with respect to the same diameter of thermocouple wires), it is more favourable to use thermocouple NiCr-NiAl.

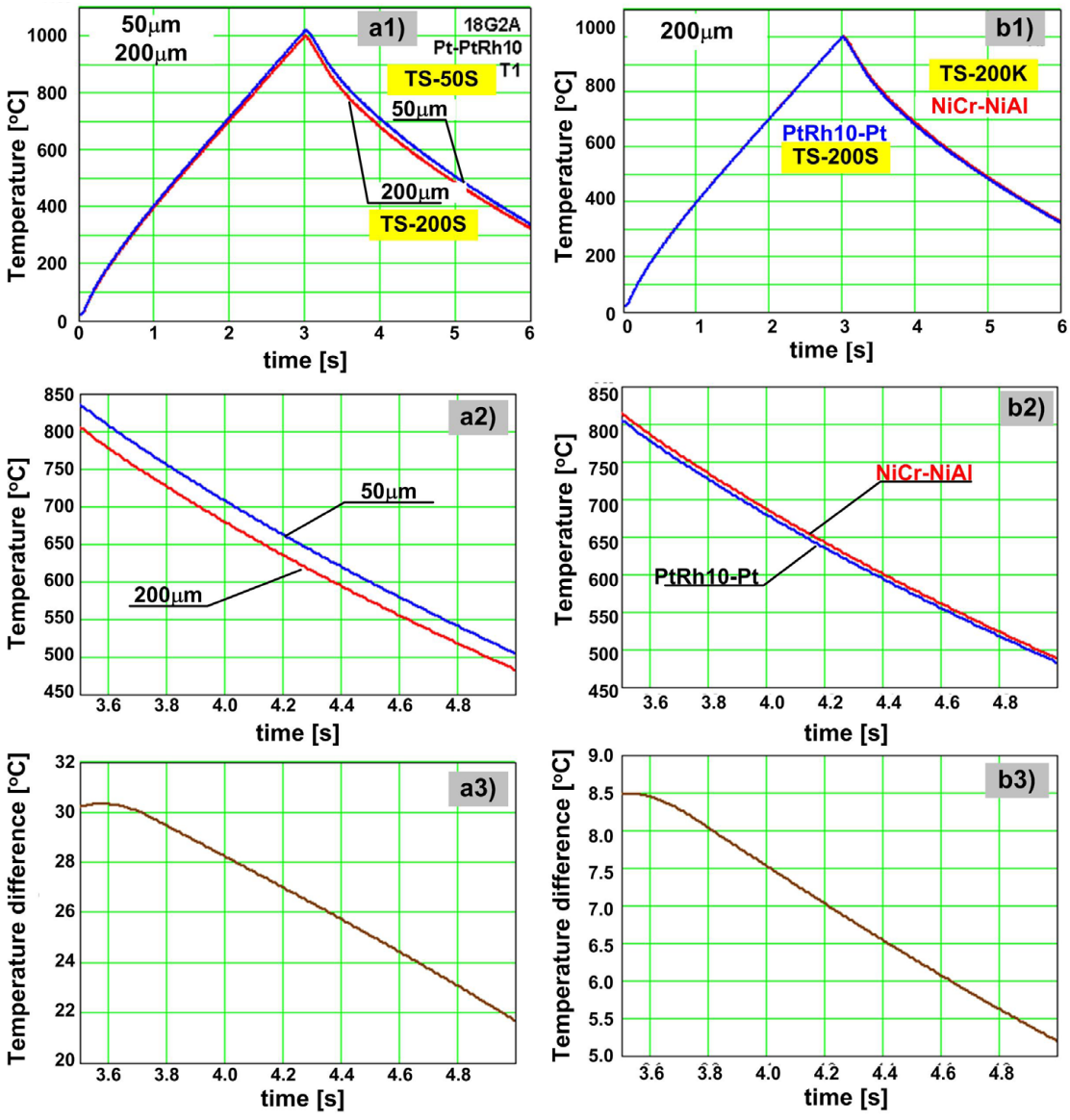

Fig. 8. Analysis of temperature distribution at various configurations

Figure 9 presents the course of temperature in relation to three different thermocouple variants, i.e. (1) TV-200K, 2) TS-200K, 3) TS-50K. Temperature was analysed in the area where the thermocouple was located (welded) (i.e. T_2) and where the thermocouple was not present physically (i.e. T_3). The points subjected to analysis were located halfway up between the points of the absorption of heat emitted by the heating lamps (points 2 and 3 Fig. 5). The subsequent lines present the courses of temperature in relation to: i) entire thermal cycle, ii) maximum temperature of the cycle (magnified) and iii) $T_{8\text{-}5}$ (magnified) respectively.

The temperature distribution in the specimen (Fig. 6 and 7) revealed the easily visible decrease in temperature in the area where the thermocouple was welded to the specimen. The above-named temperature decrease resulted from the discharge of heat by the thermocouple wires and can be improved by using thermocouples having wires of smaller diameters. It should be noted that the temperature on the specimen (measured using the *VTT*) is the temperature at the top of the hemisphere formed by the molten material of thermocouple wires (T_T). In fact, this temperature is significantly lower than the actual temperature of the specimen (T). The above-named situation can be remedied by the use of *STT*, where temperature is measured directly on the surface of the specimen.

The courses (curves) of temperature presented in Figure 9 demonstrate the course of the simulated thermal cycle. It is possible to notice the difference related to the measurement of temperature near the thermocouple (point 2 Fig. 5, T_2) and where the thermocouple was not present physically (point 3 Fig. 5, but where temperature is calculated in the numerical model, T_3).

The tests led to the determination of differences of temperature measurement (points 2 and 3 Fig. 5) in relation to the maximum temperature of the cycle (Fig. 9a2,b2,c2) and in the $T_{8\text{-}5}$ (Fig. 9a3,b3,c3) in relation to three various thermocouple variants. The above-named differences amounted to 80°C, 40°C and 2°C as well as 100°C, 50°C and 12°C respectively in relation to the maximum temperature of the cycle (1250°C) and in the $T_{8\text{-}5}$.

The numerical calculation results indicated the existence of several important factors enabling more accurate measurements (higher indications) of temperature in the conditions of a dynamic measurement (used in the testing methodology developed to perform weldability tests of materials).

The above-named factors include: i) shape (type) of the thermocouple (VTT, STT), ii) diameter of the thermocouple wires and iii) thermocouple material (in particular the heat conductivity of thermocouple wires).

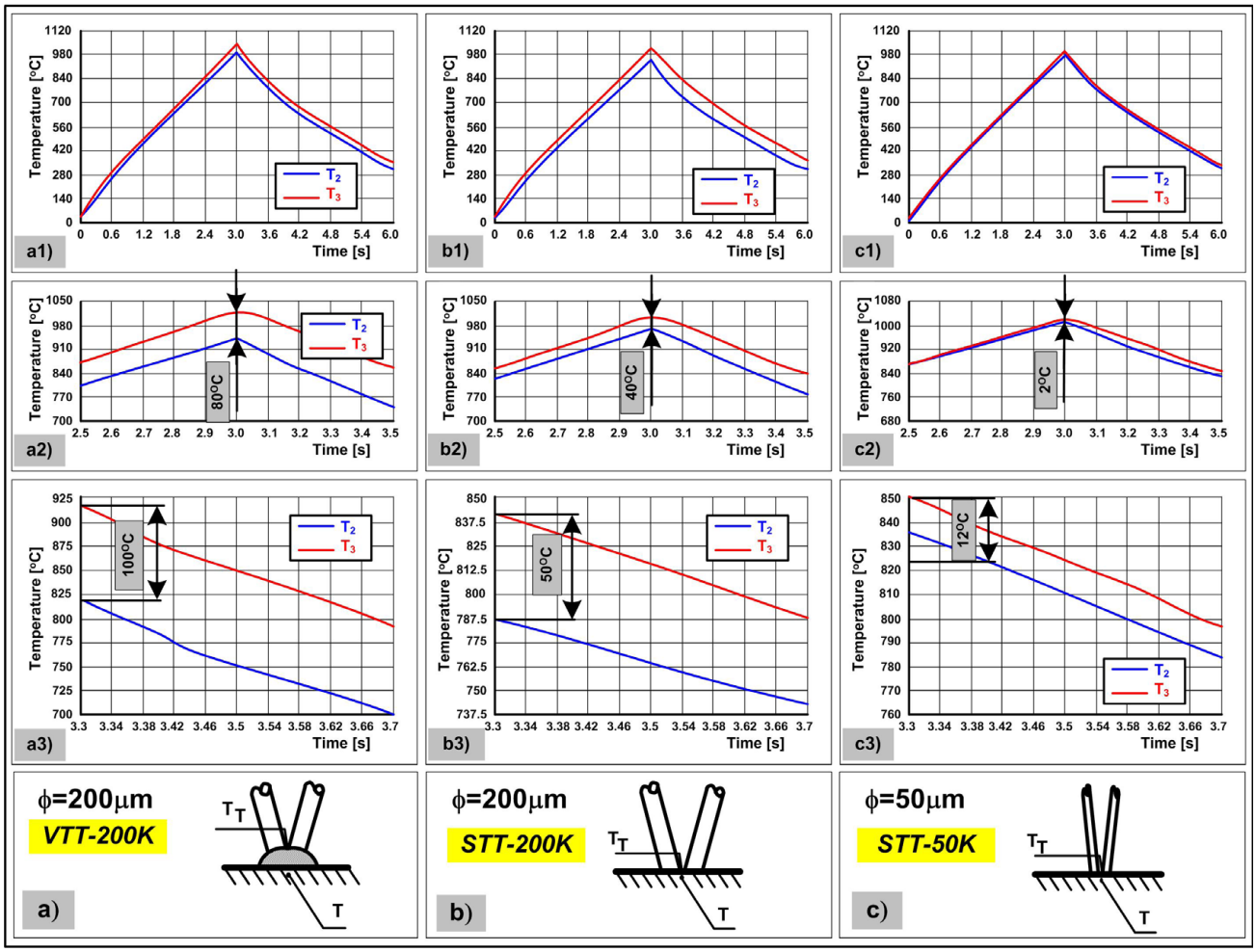

Fig. 9. Courses of temperature at points no. 2 and 3 (Fig. 5) of the specimen in relation to various types and diameters of thermocouple wires

In relation to the above-presented factors, higher accuracy of temperature measurements can be obtained by using: i) STT type thermocouples instead of VTT type thermocouples, ii) smaller diameters of thermocouple wires and iii) e.g. K type thermocouples (NiCr-NiAl) instead of S type thermocouples (PtRh10-Pt), because of lower heat conductivity).

4. Experimental verification and comparison

Tests verifying the calculations were performed using the target test rig (i.e. the one for the identification of structural transformations) [1] where two thermocouples were welded to the test specimen (subjected to heating and cooling thermal cycles).

Verification tests were performed in relation to surface thermocouples having a diameter of 200, 100 and 50 µm (TS-200K / TS-100K / TS-50K) respectively.

The verification tests (presented in the article) were performed in relation to two types of thermocouples: TS-200K and TS-50K. A comparison of temperature indications was performed in characteristic areas, i.e. for the maximum temperature value obtained in relation to a given cycle (Fig. 10a1-a2) and the maximum voltage induced because of the change in magnetic permeability (Fig. 10b1-b2).

The thermocouples were located (welded) on the opposite sides of the specimen, halfway up the specimen height, between the points of the absorption of heat emitted by the heating lamps. The courses (curves) of temperature are presented in Figure 10.

Regarding the maximum temperature of the cycle, the indications related to the thermocouple TS-50K amounted to 1306°C, whereas the indications related to the thermocouple TS-200K amounted to 1250°C; the difference between the above-presented indications amounted to 56°C (Fig. 10).

During cooling, the temperature indications amounted to 291°C and 330°C respectively. The selected temperature values correspond to the maximum values of induced voltage. It enabled the precise determination of temperatures, where the differences reached approximately 40°C. The experiment results (Fig. 10) confirmed the simulation results presented in Figure 9.

The results of the experimental tests confirmed the higher accuracy of temperature measurements (higher indications) in relation to: i) STT thermocouples instead of the VTT, ii) smaller diameter of the thermocouple wires and iii) K type thermocouples (NiCr-NiAl) instead of S type thermocouples (PtRh10-Pt).

At first, the thermocouple, being in contact with the material (the temperature of which is measured) discharges heat from the measurement area and, afterwards, performs the measurement of temperature. As in thermocouple-based measurements, the minimisation of heat discharge from the measurement area is of great importance.

As a result of the FEM calculations and experiments, the use of the volume thermocouple was abandoned as the worst solution, not worth optimising (Fig. 4).

5. Summary

The above-presented temperature measurement methodology and test rig was developed especially for the purposes of tests concerning the properties of steel specimens in simulated welding thermal cycles. Results obtained in such tests are used directly in welding engineering when developing austenite decomposition-related *CCT* diagrams (for welding conditions).

The numerical calculations and the experimental measurements of temperature made it possible to determine the uncertainty of thermocouple-based temperature measurements

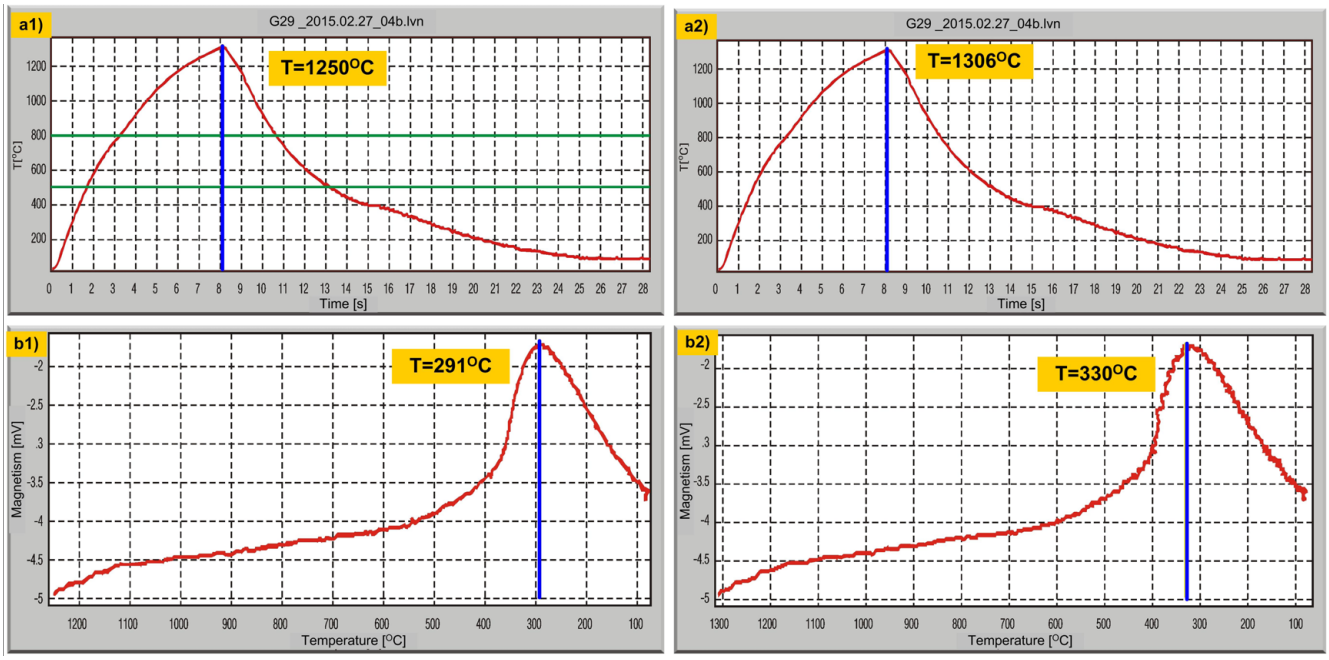

Fig. 10. Courses of: temperature (a1, a2) and induced voltage (b1, b2) in relation to the surface thermocouples having wire diameters amounting to 200 mm (a1, b1) and 50 mm (a2, b2); $t_{8/5}$ about 2.5 sec

and enabled the formulation of several interesting conclusions significantly improving the accuracy of temperature measurements:

– during dynamic temperature measurements (required in the above-presented measurement methodology) it is necessary to avoid the use of the *VTT*,
– use of the *STT* and the decrease in the thermocouple wire diameter significantly improves the accuracy of temperature measurements,
– use of a thermocouple wire material characterised by the lowest thermal conductivity (e.g. the use of the K-type thermocouple instead of the S-type, (where the range of temperatures to be measured allows for it) improves the accuracy of temperature determination.

The lowest temperature measurement uncertainty was observed in cases of short cooling times (in seconds). In cases of cooling times ($t_{8\text{-}5}$ = 3 sec.), the difference of temperature indications amounted to approximately 90°C, i.e. between the indication obtained by the *STT* having a wire diameter of 50 mm and the *VTT* having a wire diameter of 200 mm.

Acknowledgments

This work was supported by the Ministry of Science and Higher Education (MNiSW) under project no. N505 002 31/0255

REFERENCES

[1] M. Łomozik, New methodology of testing phase transformations in structural steels in welding thermal conditions, Metallic Materials - Kovove Materialy **50**, 2, 97-105 (2012).
[2] Yoshinori Ito, Kiyoshi Bessyo, Weldability formula of high strength steels related to heat affected zone cracking, IIW Document No. IX-576-68 (1968).
[3] Robert W. Messler, Principle of welding. Process, Physics, Cemistry and metallurgy" (New York, John Wiley and Sons Inc., 1999), 577-590.
[4] M.St. Węglowski, M. Zeman, Prevention of cold cracking in ultra-high strength steel Weldox 1300. Archives of Civil and Mechanical Engineering **14**, 3, 417-424 (2014).
[5] M.St. Węglowski. M. Zeman, M. Łomozik, Physical Simulation of Weldability of Weldox 1300 Steel. Materials Science Forum **762**, 551-555. (2013).
[6] M.St. Węglowski. M. Zeman, A. Grocholewski, Effect of welding thermal cycles on microstructure and mechanical properties of simulated heat affected zone for a Weldox 1300 ultra-high strength alloy steel. Archives of Metallurgy and Materials **61**, 1, 127-132 (2016).
[7] R. Branco, High-strength steels: new trends in production and applications. High strength quenched and tempered steels – weldability and welding. Nova Science Publishers. Hauppauge, Nowy Jork, USA, 2018.
[8] K. Perzynski, Ł. Madej, A. Szajding, K. Raga, K. Kubiak, A. Niechajowicz, K. Jaskiewicz, Z. Gronostajski, M. Pietrzyk, Numerical Evaluation of Gear Ring Behavior During Various Cooling Conditions, Journal of Machine Engineering **16**, 2, 18-26 (2016).
[9] F. G. Caballero, M. J. Santofimia, C. Garcia-Mateo and C. Garcia de Andres, Time-Temperature-Transformation Diagram within the Bainitic Temperature Range in a Medium Carbon Steel, the Japan Institute of Metals, Materials Trans. **45**, 12, 3272-3281 (2004)
[10] W. Bendick, J. Gabriel, B. Hahn, B. Vandenberghe, International Journal of Pressure Vessels and Piping **84**, 13-20 (2007).
[11] H. Bhadeshia Lecture 10: Overall Transformation Kinetics II. Course MP6, Kinetics and Microstructure Modelling. Materials Science & Metallurgy Master of Philosophy, Materials Modelling. Cambridge University 2003.
[12] M. Kasprzak, W. Kasprzak, W. Kierkus, J. Sokolowski, Applications of High Frequency Induction Heating for the Metallurgical Simulation and Thermal Analysis of Industrial Light Metals Casting Processes, Proc. of 2002 TMS Annual Meeting, The Minerals, Metals & Materials Society, 2002 Seattle, Washington, USA, Feb.17-21, 2002, pp.619-630.
[13] A. Gesing, J. Sokolowski, P. Marchwica, C. Blawert, J. Jekl, M. Kozdras, M. Kasprzak, J. Wood, Cooling curve and microchemical phase analysis of rapidly quenched magnesium AM60B and AE44 alloys, Proc. of Achievements in Mechanical and Materials Engineering, AMME'2013, Gliwice – Kraków, 2013, pp.75-76.
[14] J. C. Lippold, Welding Metallurgy and Weldability, 2015, John Wiley & Sons.
[15] G. M. Boyd, Brittle Fracture in Steel Structures, London Butterworths for Navy Department Advisory Committee on Structural Steel, Elsiver 2016.
[16] R. Thomas, G. Morgan, 1992, Measurement of Magnetic Permeability and HC of Magnet Steels using Digital Techniques. Brookhaven National Laboratory Upton, New York.
[17] Z. Mikno, M. Łomozik, M. Zeman, A. Pilarczyk, A manner and bench to determinate characteristic points of structural transformations in steels in thermal welding cycles, Polish Patent no Pat.218257.
[18] M. Łomozik, A. Pilarczyk, TPF 3.0 to create diagrams of austenite phase transformations in steels under welding conditions (CCT), Przegląd Spawalnictwa **3**, 23-27 (2012).
[19] Z. Mikno, M. Stępień, B. Grzesik, Test bench to prepare thermocouple junction to temperature measurements in small size elements, Polish Patent no Pat.215566.
[20] J. Słania, Z. Mikno, M. Wójcik, Selected problems of temperature measurement in welding processes, Advances in Manufacturing Science and Technology 3, 83-93.(2007).
[21] L. Michalski, K. Eckersdorf, Temperature measurement (in Polish), WNT Warszawa 1986.
[22] L. Kortvelyessy, Termoelement Praxis Vulkan-Verlag-Essen 1987.
[23] Z. Mikno, Project report KBN nr 4T08C 006 24, Gliwice 2004 (unpublished).
[24] Z. Mikno, B. Grzesik, M. Stępień, Project report NCN N505 002 31/0255, Gliwice 2009 (unpublished).